

# Independent-electron analysis of the x-ray spectra from single-electron capture in $\text{Ne}^{10+}$ collisions with He, Ne, and Ar atoms

Anthony C. K. Leung\* and Tom Kirchner†

*Department of Physics and Astronomy, York University, Toronto, Ontario M3J 1P3, Canada*

(Received 8 July 2015; published 23 September 2015)

We present a theoretical study on the x-ray spectra from single-electron capture in 4.54 keV/amu  $\text{Ne}^{10+}$ -He, -Ne, and -Ar collisions. Single-particle capture probabilities were calculated using the two-center basis generator method within the independent electron model. In this framework we investigated the effects of a time-dependent screening potential that models target response on capture cross sections and x-ray spectra. Excellent agreement is shown with the previously measured relative cross sections and x-ray spectra and calculations based on the classical trajectory Monte Carlo method using the no-response single-particle electron capture probabilities in a multinomial single-electron capture analysis. Our results demonstrate the importance of using this consistent statistical analysis of single-electron capture within the independent electron model; a requirement that a previous calculation for the same collision problem using the two-center atomic-orbital close-coupling method may not have considered.

DOI: [10.1103/PhysRevA.92.032712](https://doi.org/10.1103/PhysRevA.92.032712)

PACS number(s): 34.50.Fa, 34.70.+e

## I. INTRODUCTION

In the past decade x-ray emissions have been the subject of great interest from an astrophysical perspective [1–10]. They have been recognized as a characteristic in certain astronomical objects such as gases from comet tails, where these emissions are believed to originate from interactions with highly charged solar wind ions via charge exchange followed by spontaneous emission [4,6,7]. With novel measurement techniques such as cold target recoil momentum spectroscopy (COLTRIMS), where coincidence measurements can be made, one can view collision dynamics at the atomic level [1,2,11–13]. The high level of detail and precision from COLTRIMS coincidence measurements offers opportunities to test various theoretical models such as the classical trajectory Monte Carlo (CTMC) method [8–10] and quantum-mechanical close-coupling [14,15] approaches.

A triple-coincidence experiment using COLTRIMS was carried out by Ali *et al.* to obtain  $n$ -state-selective relative capture cross sections and x-ray spectra by charge transfer from 4.54 keV/amu  $\text{Ne}^{10+}$ -He, -Ne, and -Ar collisions [2]. Measurements of x-ray spectra from single-electron capture (SEC) were separated from multiple-electron capture, which allows to model the x-ray spectra for the simplest case (i.e., SEC). In the same work, SEC CTMC calculations were carried out and compared with the experimental SEC  $n$ -state selective cross sections and x-ray spectra. It was shown that the CTMC relative cross sections were in good agreement with corresponding measurements, but some discrepancies were observed in the x-ray spectra, in particular, for the  $\text{Ne}^{10+}$ -He collision system. The authors suspected that this may be due to a lack of electron correlation effects included in the CTMC model.

A recent theoretical study of He and Ne targets was performed by Liu *et al.* using the two-center atomic-orbital close-coupling (TC-AOCC) method within the independent electron model (IEM) [15]. It was found that TC-AOCC calculations of

the  $n$ -state-selective relative capture cross sections were not on the same level of agreement with cross-section measurements by Ali *et al.* [2] but do show slight improvements on certain Lyman peaks in the x-ray spectra compared to CTMC. Liu *et al.* speculated that the large discrepancies in the relative cross sections from those of Ali *et al.* [2] may be due to the model potential used in the Hamiltonian. There was also speculation on the neglect of two- or multiple-electron capture as another source of the discrepancy. However, this would not match the experimental protocols of Ali *et al.* [2], who, as previously mentioned, separated SEC cross sections and x-ray spectra measurements from multiple-electron capture, which is a feature of a COLTRIMS coincidence experiment.

Solving the time-dependent Schrödinger equation (TDSE) of a many-electron system using the IEM yields single-particle solutions. By projecting these solutions onto appropriate final states one obtains single-particle probabilities for either capture, ionization, or target excitation. For an accurate physical representation one combines the single-particle probabilities using a multinomial analysis [16–18]. This statistical approach has been applied successfully in previous collision studies involving multiple-electron processes [19–21]. Although Liu *et al.* [15] used a binomial equation for an analysis of single- and double-electron capture probabilities, it is not clear if this was implemented in the capture cross-section calculations that were used for the x-ray spectra analysis. Given these inconsistencies and the fact that the  $\text{Ne}^{10+}$ -Ar system was not addressed in Ref. [15], there is considerable motivation to extend and complete the discussion of the collision problems reported by Ali *et al.* [2] in the framework of the IEM.

In this paper, we report an independent-electron analysis of the x-ray spectra study reported in Ref. [2] using the two-center basis generator method (TC-BGM) [22]. The TC-BGM and the IEM used as well as the modeling of x-ray spectra are described in Sec. II. In Sec. III, we present the SEC capture cross sections and x-ray spectra calculated in this framework and compare results with previous studies [2,15]. Finally in Sec. IV, we provide our concluding remarks. Atomic units ( $\hbar = e = m_e = 4\pi\epsilon_0 = 1$ ) are used throughout the paper unless stated otherwise.

\*leungant@yorku.ca

†tomk@yorku.ca

## II. THEORY

The problem of interest is a bare  $\text{Ne}^{10+}$  projectile colliding with a He, Ne, or Ar target at 4.54 keV/amu (933 km/s). This collision energy is said to correspond to the higher end of solar wind ion velocities [2]. With one electron captured into an excited state of the projectile it then decays to the ground state by spontaneous emission.

### A. Collision description

For all collision systems we solve the single-particle TDSE using the IEM within the semiclassical approach. Here, we describe the single-particle Hamiltonian by

$$\hat{H}(t) = -\frac{1}{2}\Delta - \frac{Z_T}{r} - \frac{Z_P}{|\mathbf{r} - \mathbf{R}(t)|} + v_{ee}(\mathbf{r}, t), \quad (1)$$

where  $Z_T$  and  $Z_P$  are the charges of the target and projectile nuclei, respectively. In the semiclassical approach the projectile is assumed to follow a straight-line path at constant speed  $v_p$  described by  $\mathbf{R}(t) = (b, 0, v_p t)$ , where  $b$  is the impact parameter. Furthermore, Hamiltonian (1) includes an effective single-particle potential  $v_{ee}$  that models the electron-electron interaction and we consider two variants: (a) the no-response approximation, where an atomic ground-state potential obtained from the optimized potential method of density functional theory [23] is used; and (b) a target response model, in which a spherical time-dependent screening potential is also included. These approximations were investigated in previous studies [19,20], and it was found that the target response mechanism has an important role in the low- to intermediate-energy regime in estimating capture and ionization cross sections.

We solve the TDSE for Hamiltonian (1) using the coupled-channel TC-BGM [22,24]. For this collision study we include all possible states of the  $KLMN$  shells for He and Ne, all possible states of the  $LMN$  shells for Ar, hydrogen-like states from  $n = 1$  to  $n = 10$  on the projectile, and a set of BGM pseudostates. Although the BGM pseudostates account for intermediate quasimolecular couplings and for transitions to the continuum, they were in fact found to be of minor importance in the present study because of the strong dominance of capture transitions.

From the TC-BGM calculations we obtain  $nl$ -state-selective single-particle capture probabilities  $p_i^{\text{cap}}(n, l)$  and ionization probabilities  $p_i^{\text{ion}}$ , a multinomial combination of which yields probabilities for  $q$ -fold capture with simultaneous  $k$ -fold ionization  $P^{qk}$  [16–18]. In this study we are interested in single capture and no ionization (i.e.,  $q = 1$  and  $k = 0$ ), so we designate  $P_{nl}^{10}$  the subshell-specific SEC probability

$$P_{nl}^{10} = \sum_{q_1, \dots, q_m} \prod_{i=1}^m \binom{N_i}{q_i} (p_i^{\text{cap}}(n, l))^{q_i} \times (1 - p_i^{\text{cap}} - p_i^{\text{ion}})^{N_i - q_i} \delta_{1, \sum_i q_i}, \quad (2)$$

where  $m$  is the number of electron orbitals in the target atom,  $N_i$  is the number of electrons in the  $i$ th orbital ( $N_i = 2$ , for all  $i$ ), and  $p_i^{\text{cap}} = \sum_{n, l} p_i^{\text{cap}}(n, l)$ .

In addition to SEC probabilities we consider net capture,

$$P_{nl}^{\text{net}} = 2 \sum_i^m p_i^{\text{cap}}(n, l), \quad (3)$$

which, because of the relation [25–27]

$$P_{nl}^{\text{net}} = \sum_{q, k} q P_{nl}^{qk}, \quad (4)$$

can be interpreted as the average number of captured electrons. It is noteworthy that for low single-particle probabilities, multielectron capture ( $P^{qk}$  with  $q \geq 2$ ) becomes negligibly small and expression (2) essentially reduces to the net capture, (3).

With the combined capture probabilities we calculate  $nl$ -state-selective capture cross sections

$$\sigma_{nl} = 2\pi \int_0^\infty b P_{nl}(b) db \quad (5)$$

for both SEC and net capture. It is clear that (2) gives a consistent representation of the SEC cross sections within the IEM, while the net capture, (3), is contaminated by multiple-capture events, which may be significant for a highly charged projectile ion.

### B. Cascade modeling

In this study the projectile is a bare  $\text{Ne}^{10+}$  and becomes a hydrogen-like ion when an electron is captured into an excited state. The electron then decays to the lowest energy state and the decay was assumed to follow the electric dipole selection rule (i.e.,  $\Delta l = \pm 1$ ). Then the rate of population  $N_{nl}(t)$  of a particular  $nl$  state is

$$\frac{dN_{nl}}{dt} = \sum_{\substack{n''=n+1; \\ |l-l''|=1}}^\infty N_{n''l''}(t) A_{n''l'' \rightarrow nl} - N_{nl}(t) \sum_{\substack{n'=1; \\ |l-l'|=1}}^{n-1} A_{nl \rightarrow n'l'}, \quad (6)$$

where the first sum on the right-hand side of (6) is the repopulation rate from higher  $n''l''$  states with transition rate  $A_{n''l'' \rightarrow nl}$  and the second sum is the depopulation rate to lower  $n'l'$  states with transition rate  $A_{nl \rightarrow n'l'}$ . The transition rates shown in (6) can be calculated analytically for the case of hydrogen-like  $\text{Ne}^{9+}$ . Starting from the general expression for the spontaneous emission rate in the dipole approximation [28]

$$A_{i \rightarrow f} = \frac{4}{3} \left( \frac{\omega_{if}}{c} \right)^3 |\mathbf{r}_{if}|^2, \quad (7)$$

where  $\mathbf{r}_{if}$  is a dipole matrix element, and using the Wigner-Eckart theorem we obtain

$$A_{nl \rightarrow n'l'} = \frac{4}{3} \left( \frac{\omega_{nn'}}{c} \right)^3 (2l' + 1) \begin{pmatrix} l' & 1 & l \\ 0 & 0 & 0 \end{pmatrix}^2 \times \left( \int_0^\infty R_{nl} R_{n'l'} r^3 dr \right)^2, \quad (8)$$

where  $\omega_{nn'}$  is the transition frequency and  $R_{nl}$  is the radial wave function for hydrogen-like  $\text{Ne}^{9+}$ . Once the populations  $N_{nl}(t)$  are obtained we proceed to calculate the total photon counts by integrating the simple intensity expression [29]

$$\text{counts} = A_{nl \rightarrow n'l'} \int_0^\infty N_{nl}(t) dt. \quad (9)$$

In this study we are only interested in integrating those  $N_{nl}(t)$  that contribute to the Lyman spectrum (i.e.,  $n \geq 2 \rightarrow n = 1$  transitions).

### III. RESULTS AND DISCUSSION

#### A. Capture probabilities and cross sections

We first recall from Sec. II A that the net capture, (3), can deviate from SEC, (2), considerably if the single-particle capture probabilities are higher than a few percent. As a demonstration, Fig. 1 shows the TC-BGM net capture and SEC results over the impact parameter for the  $\text{Ne}^{10+}$ -Ne collision system. The figure clearly shows the stark differences in magnitude between SEC probabilities and net capture. Moreover, the range of impact parameters indicating where capture is most probable appears much narrower in the SEC plots than the net capture ones. The present TC-BGM single-particle capture probabilities were, in fact, found to be high enough over a range of impact parameters that led to  $P_n^{\text{net}} > 1$  [e.g., Figs. 1(a) and 1(b)]. This demonstrates that multielectron capture is strong in this collision system.

In the work by Ali *et al.* [2] it was shown that  $n = 5$  is the dominant SEC channel for the  $\text{Ne}^{10+}$ -Ne collision system. By comparing the panels in Fig. 1, it is very clear that the SEC probability plots indicate that the  $n = 5$  capture channel has the largest area under the curve, implying by far the largest capture cross section, (5), compared to the two subdominant channels. In the case of net capture plots, things are not as straightforward. Nevertheless, capture cross sections from net capture are considered as well in the following in order to draw proper comparisons not only with the present SEC results but also with Liu *et al.* [15] and Ali *et al.* [2].

The partial electron-capture cross sections  $\sigma_{nl}$  for  $n = 3$  to  $n = 7$  shells from the present TC-BGM no-response approximation along with the results of Liu *et al.* [15], which have been obtained within a similar framework, are listed in Table I. The present TC-BGM  $\sigma_{nl}$  values in the target response approximation are listed in Table II (Appendix A). In the work by Ali *et al.* [2] it was shown that  $n = 5$  is the dominant capture channel for  $\text{Ne}^{10+}$ -He and -Ne collisions, while  $n = 6$  is the dominant channel for  $\text{Ne}^{10+}$ -Ar collisions. We see that the present  $\sigma_{nl}$  values listed in Table I are consistent with the results measured by Ali *et al.* [2].

It is clearly shown in Table I that the various TC-BGM  $\sigma_{nl}$  and those of Liu *et al.* [15] differ from one another. For the  $\text{Ne}^{10+}$ -He system, the present TC-BGM net  $\sigma_{nl}$  values are roughly a factor of 2 greater than the Liu *et al.* values. We recall that the net capture expression for this collision system is simply given by  $P_{\text{net}} = 2p_{\text{cap}}$  since there is only one occupied shell in He. One implication of this observation is that the  $\sigma_{nl}$  reported by Liu *et al.* [15] may correspond to the single-particle capture probabilities. However, there is no consistent pattern

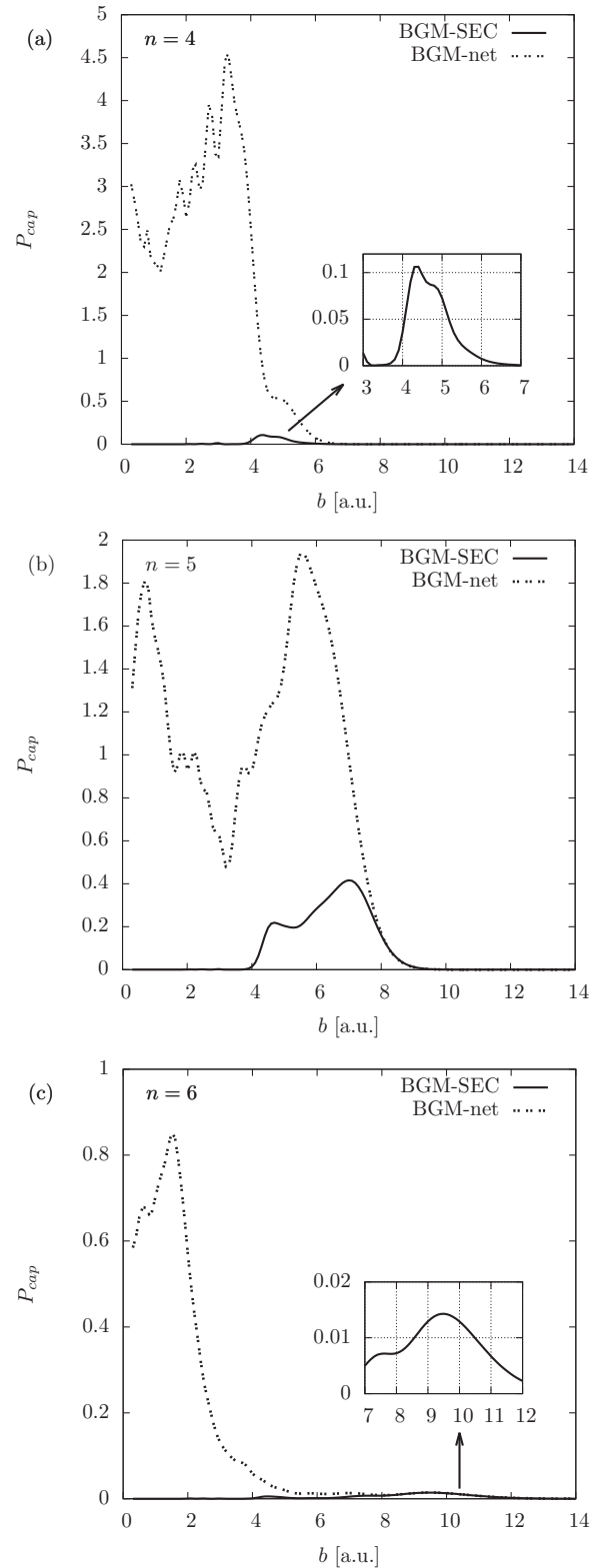


FIG. 1. TC-BGM SEC probabilities and net capture to the (a)  $n = 4$ , (b)  $n = 5$ , and (c)  $n = 6$  shells of the projectile in  $\text{Ne}^{10+}$ -Ne collisions at  $E_p = 4.54$  keV/amu. Calculations correspond to the no-response approximation.

for the  $\text{Ne}^{10+}$ -Ne collision system to deduce how the results in Ref. [15] relate to expression (2) or (3) in the present study.

TABLE I. Partial cross sections  $\sigma_{nl}$  (in  $10^{-16}$  cm<sup>2</sup>) from the TC-BGM no-response approximation and from Liu *et al.* [15].

States ( $n, l$ )	Ne <sup>10+</sup> -He			Ne <sup>10+</sup> -Ne			Ne <sup>10+</sup> -Ar	
	Liu <i>et al.</i> [15]	Net	SEC	Liu <i>et al.</i> [15]	Net	SEC	Net	SEC
3,0	0.00259	0.006	0.0059	0.11334	0.988	$8.9 \times 10^{-5}$	0.0814	$6.4 \times 10^{-8}$
3,1	0.00497	0.013	0.00120	0.38767	2.580	0.000176	0.115	$1.6 \times 10^{-8}$
3,2	0.00555	0.014	0.00122	0.43212	2.639	0.00018	0.164	$7.1 \times 10^{-9}$
4,0	1.28001	2.702	0.655	0.61863	4.080	0.1209	3.254	0.00028
4,1	2.49743	5.312	1.424	1.54824	12.337	0.2606	7.918	0.00070
4,2	2.3663	5.074	1.316	2.20899	20.443	0.3469	9.986	0.00068
4,3	1.65268	3.610	0.831	2.27206	19.955	0.3137	8.611	0.00046
5,0	0.40824	0.793	0.518	0.4479	2.055	0.9694	7.106	0.090
5,1	1.59903	2.875	1.846	1.26065	6.480	1.7530	20.021	0.195
5,2	3.3875	6.097	3.730	1.89889	12.969	3.0252	28.942	0.230
5,3	5.19333	9.352	5.097	2.06158	19.746	3.7898	40.350	0.205
5,4	5.59273	10.123	4.953	1.79232	22.255	3.0958	37.188	0.123
6,0	0.01865	0.032	0.005	0.08522	0.128	0.0131	3.013	0.989
6,1	0.06549	0.116	0.018	0.83357	0.291	0.0299	9.367	1.947
6,2	0.13175	0.213	0.033	1.07244	0.808	0.0673	20.175	3.636
6,3	0.16082	0.269	0.047	1.05582	1.729	0.1311	31.090	5.001
6,4	0.22599	0.399	0.083	0.65926	1.050	0.2403	42.191	4.894
6,5	0.46632	0.783	0.219	0.63372	1.725	0.3650	45.392	3.127
7,0	0.00124	0.004	0.001	0.08617	0.019	0.0001	0.279	0.054
7,1	0.0089	0.013	0.002	0.75998	0.080	0.0002	0.854	0.115
7,2	0.01096	0.016	0.003	0.94827	0.103	0.0002	1.759	0.269
7,3	0.01814	0.030	0.004	0.85963	0.145	0.0003	2.626	0.557
7,4	0.04396	0.077	0.011	0.57296	0.271	0.0007	3.800	1.060
7,5	0.03353	0.045	0.009	0.30936	0.276	0.0011	5.509	1.830
7,6	0.00814	0.014	0.004	0.09185	0.165	0.0037	7.613	2.203

Liu *et al.* [15] noted that they included, in total, four bound states on the Ne atom in their calculation, namely, the  $2p$  and  $3p$  states. This raises some concerns for the following reasons. First, the  $2p$  and  $3p$  subshells consist of three states each, either of the standard  $p_{-1}$ ,  $p_0$ ,  $p_1$  states corresponding to complex spherical harmonics or of states that correspond to real spherical harmonics and preserve a mirror symmetry of the Hamiltonian, (1), which makes them a popular choice in close-coupling scattering calculations. Second, it appears problematic to exclude the  $s$  and  $d$  subshells, thereby blocking dipole-like transitions. By revisiting our TDSE calculation using the TC-BGM for the Ne<sup>10+</sup>-Ne collision system we found that excluding the Ne  $2s$  and  $3s$  states yields noticeable differences in the capture cross sections compared to the original TC-BGM calculation with the full basis; for example, the cross sections for the dominant capture channel  $n = 5$  do not appear as prominent as those in Table I.

In a different perspective we show the relative weightings of the partial capture cross sections  $s_{nl} = \sigma_{nl}/\sigma_n$  for the dominant and subdominant capture channels in Fig. 2. All present TC-BGM results and those of Liu *et al.* [15] are included. In most cases the relative  $l$  distributions correspond to the statistical relation [i.e.,  $\propto (2l + 1)$ ], where electrons are mostly captured in the maximum  $l$  subshell. There are other instances where electrons appear to be mostly populated in the low- $l$  subshells [e.g., Fig. 2(a) for  $n = 4$ ]. Moreover, we note the similar relative  $l$  distributions between the results of Liu

*et al.* [15] and the present TC-BGM results in the no-response approximation for the Ne<sup>10+</sup>-He collision system [Fig. 2(a)]. Comparing the various present TC-BGM calculations, the influence of the response approximation or the net capture and SEC comparison of the relative  $l$  distributions do not appear to have a clear pattern for each collision system.

The  $n$ -state-selective relative cross sections  $\sigma_n^{\text{rel}} = \sigma_n/\sigma_{\text{total}}$  for the present TC-BGM calculations are shown in Fig. 3 and listed in Table III (Appendix A). We compare the TC-BGM net results with those of Liu *et al.* [15] in Fig. 3(a), while we compare the TC-BGM SEC results with those of CTMC calculations by Ali *et al.* [2] in Fig. 3(b). The experimental  $\sigma_n^{\text{rel}}$  values of Ali *et al.* [2] shown in both panels have a sharp peak for each collision system which illustrates the dominant capture channel. We see in Fig. 3(b) that the TC-BGM no-response approximation using the SEC expression, (2), is on the same level of agreement with the experiment as the CTMC. While the present TC-BGM net capture  $\sigma_n^{\text{rel}}$  also shows the correct trend with the experimental  $\sigma_n^{\text{rel}}$ , there are noticeable contributions ( $> 10\%$ ) from low- $n$  channels compared to the other calculations, which leads to a lower percentage contribution in the dominant channel. A similar observation also applies to the results of Liu *et al.* [15]. Although the present TC-BGM net  $\sigma_n^{\text{rel}}$  values do not agree well with the measurements for the lower subdominant capture channels, it is interesting to see that the net cross sections agree well with the higher subdominant

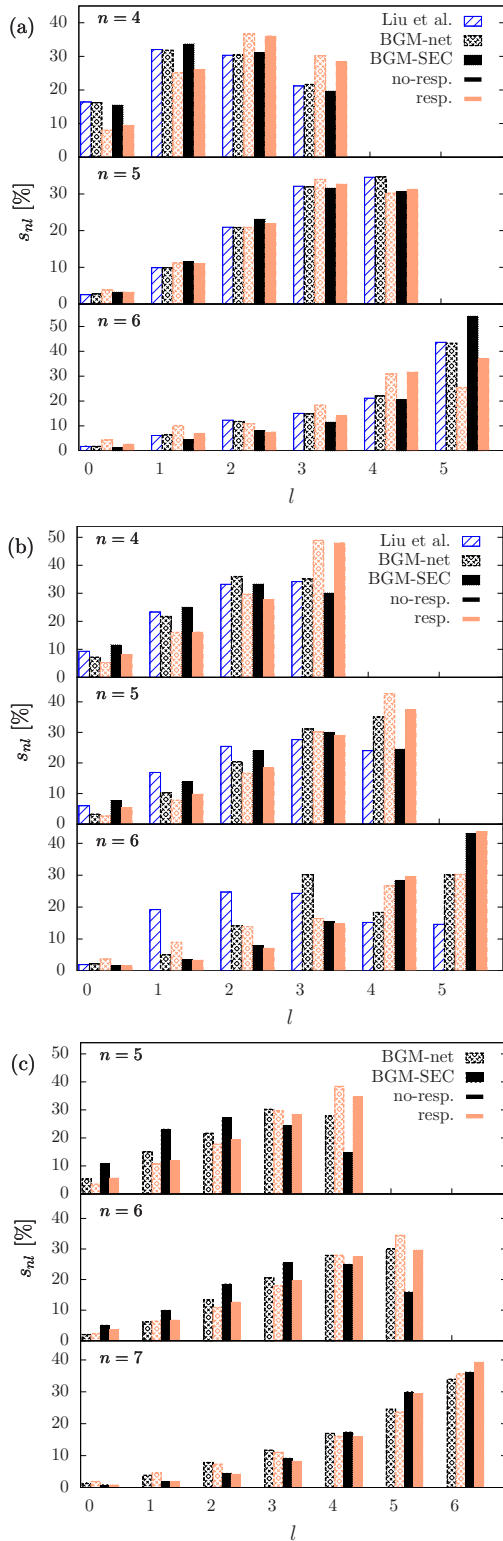


FIG. 2. (Color online) Weighted partial cross section  $s_{nl}$  distributions for  $\text{Ne}^{10+}$  collisions with (a) He, (b) Ne, and (c) Ar.  $s_{nl}$  distributions for Liu *et al.* are calculated using the data from Ref. [15] as reproduced in Table I.

channels for all collision systems (e.g.,  $n = 7 + 8$  in  $\text{Ne}^{10+}$ -Ar collisions).

In general, our target response calculations do not appear to give a better estimation of the  $\sigma_n^{\text{rel}}$  than the no-response

approximation. As shown in Fig. 3 the tendency of the target response approximation is similar to that of the net capture analysis. Although previous studies on multiple-electron capture have shown that including the target response model may improve the cross-section results [21], the present study on SEC shows the contrary. However, this observation is not inconsistent with what was noted in Ref. [19], namely, that capture at low impact energies probes the specific form of the response potential and that a spherical model might be too crude for the present problem. Given that the projectile is a bare  $\text{Ne}^{10+}$  ion the potential field around the target nucleus, when the projectile is nearby, should show strong polarization, which is beyond the present modeling.

Through these discussions and comparisons, it is evident that the capture cross sections by Liu *et al.* [15] and the TC-BGM net capture do not reflect the SEC events that occurred in the experiment reported by Ali *et al.* [2]. Within the IEM the multinomial calculation of  $P_{nl}^{10}$  is the only suitable representation of these capture events. In the following section, x-ray emission spectra results are discussed. The x-ray spectra using the net capture cross sections and results of Liu *et al.* [15] are not considered in this discussion.

## B. X-ray emission spectra

The modeled  $n$ -state-selective hydrogen-like  $\text{Ne}^{9+}$  x-ray spectra from the He, Ne, and Ar collisions are shown in Figs. 4, 5, and 6 respectively. In each figure, the TC-BGM SEC spectrum is compared with the CTMC and experimental results of Ali *et al.* [2].

The CTMC calculations of the x-ray spectra reported by Ali *et al.* [2] were convolved to a Gaussian profile with 126-eV full width at half-maximum (FWHM) and mutually normalized to the experimental areas. Consequently, only two Gaussian peaks are observed for each  $n$ -resolved spectrum and are identified as the Ly- $\alpha$  ( $n = 2 \rightarrow n = 1$ ) and Ly- $\beta+$  ( $n \geq 3 \rightarrow n = 1$ ) peaks. For consistency, the same convolution and normalization process was applied to the present TC-BGM results. The convolution process of the x-ray lines is illustrated in Appendix B.

As shown in Figs. 4, 5, and 6 there are many similarities between all modeled spectra, with a general overestimation of the Ly- $\alpha$  and an underestimation of the Ly- $\beta+$  peaks compared to the experimental results. Similarly to the CTMC, the present TC-BGM spectra show reasonable agreement with the experimental spectra for the Ne target system (Fig. 5) and excellent agreement with the Ar target system (Fig. 6). There are also similar agreements with the CTMC for the He target system in channels  $n = 5$  and  $n = 6$ , but not for  $n = 4$ , where the present TC-BGM shows better agreement with the experimental spectrum (Fig. 4).

For the TC-BGM spectra, we see that including the target response leads to changes in the spectral peaks compared to the no-response approximation. However, these changes do not appear consistent in all channels for each collision system. In certain cases, the difference between the no-response and the response spectra are not noticeable (e.g.,  $n = 5$  in Fig. 4).

Differences in the spectral peaks, or a lack thereof, can be understood by examining the relative  $l$  distributions of the

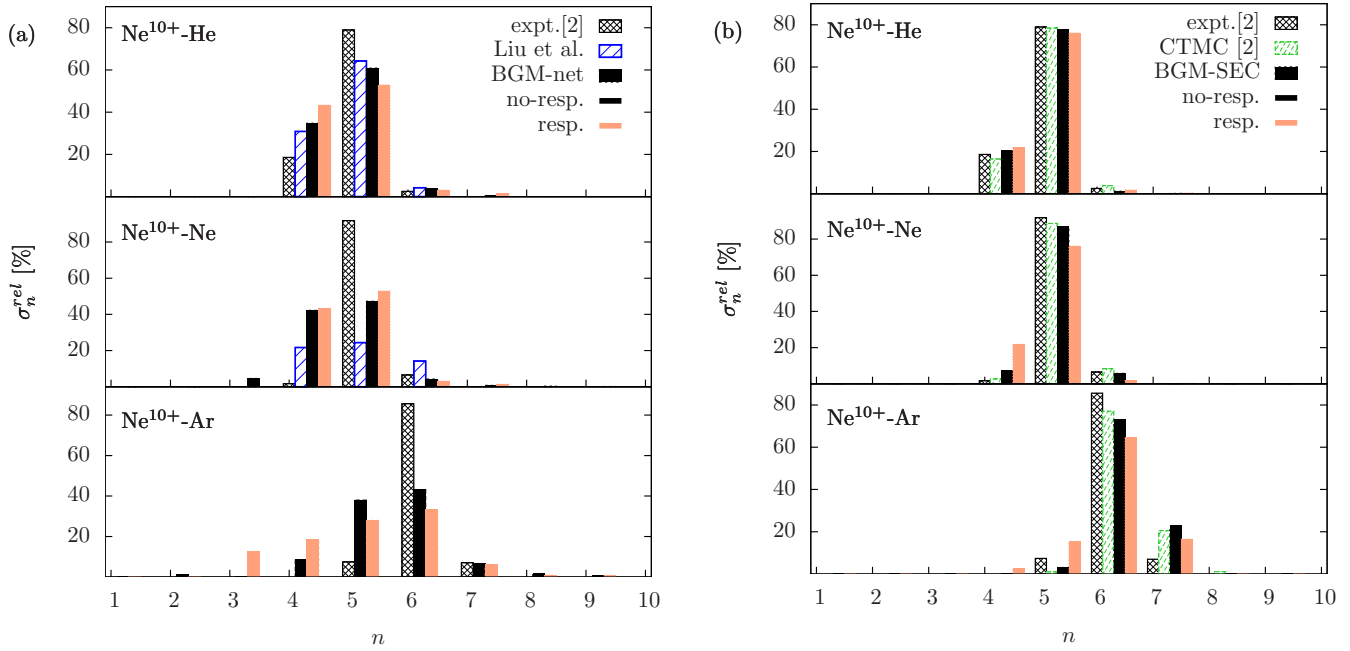


FIG. 3. (Color online)  $n$ -state selective relative cross sections  $\sigma_n^{rel}$  in the  $Ne^{10+}$ -He, -Ne, and -Ar collision systems: (a) TC-BGM net  $\sigma_n^{rel}$  with Liu *et al.* [15] and experimental data of Ali *et al.* [2]; (b) TC-BGM SEC with CTMC and experimental data of Ali *et al.* [2].

partial capture cross sections (Fig. 2). One would expect that the more similar the relative  $l$  distribution, the more similar the x-ray spectral peaks. This is indeed the case and very obvious in the  $n = 7$  channel for the  $Ne^{10+}$ -Ar collision system, where

similarities shown in Fig. 2(c) are reflected in Fig. 6. Another scenario to better understand the spectral peak heights is to compare the relative partial cross sections at the maximum  $l$  subshell. Electrons initially occupying this subshell can only

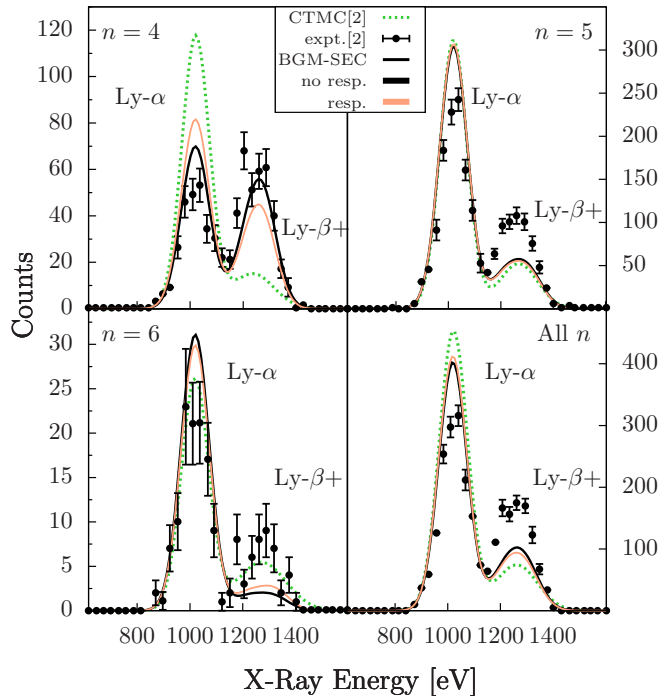


FIG. 4. (Color online) X-ray spectra from SEC in the  $Ne^{10+}$ -He collision system: TC-BGM SEC, CTMC, and spectra measured by Ali *et al.* [2].

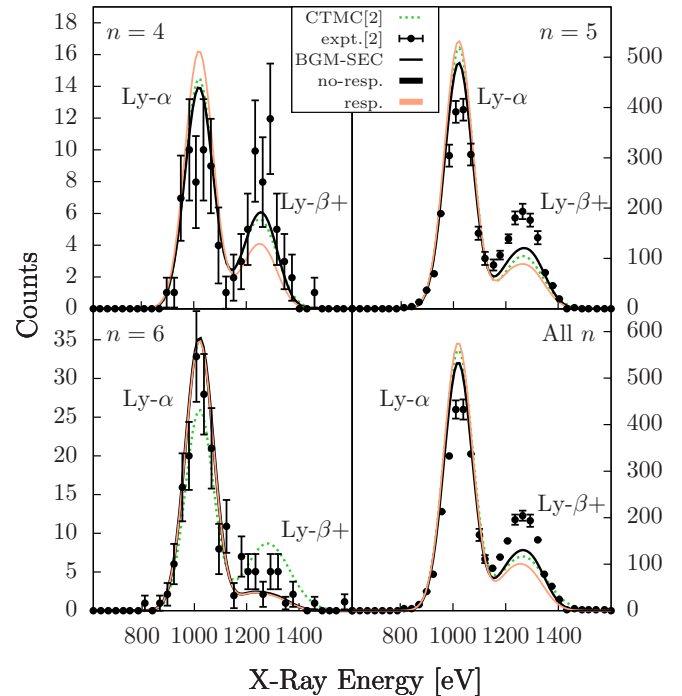


FIG. 5. (Color online) X-ray spectra from SEC in the  $Ne^{10+}$ -Ne collision system: TC-BGM SEC, CTMC, and spectra measured by Ali *et al.* [2].

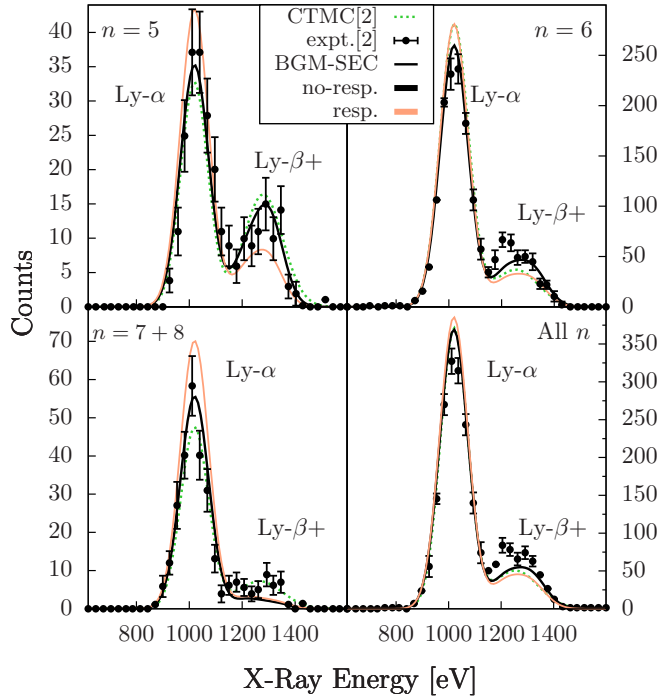


FIG. 6. (Color online) X-ray spectra from SEC in the  $\text{Ne}^{10+}$ -Ar collision system: TC-BGM SEC, CTMC, and spectra measured by Ali *et al.* [2].

follow the *yrast cascade*,

$$\dots 4f \rightarrow 3d \rightarrow 2p \rightarrow 1s,$$

which is a main contributor to the Ly- $\alpha$  peak. We again consider the  $\text{Ne}^{10+}$ -Ar collision system, but now the  $n = 5$  channel, where the relative cross section at  $l = 4$  for the TC-BGM no-response SEC calculation is the lowest [Fig. 2(c)] and consequently the Ly- $\alpha$  peak is lower compared to the TC-BGM response result (Fig. 6).

A disadvantage with the process of mutually normalizing the modeled x-ray spectra to the experimental areas shown in Figs. 4–6 is that the spectral counts of one capture channel relative to another one do not reflect the relative cross sections of the respective channels. In the present study, this normalization process led to identical area ratios between the no-response and the response models. If the  $\sigma_{nl}$  are used as initial values for the cascade model, (6), then the  $n$ -state-selective cross section ratios are preserved as spectral area ratios. Consider the  $\text{Ne}^{10+}$ -Ne collision system as an example. In Fig. 5, the ratio of areas under the TC-BGM SEC spectra (no response or response) between the  $n = 5$  and the  $n = 4$  channel is  $I(n = 5)/I(n = 4) \approx 31.1$ . The corresponding  $\sigma_n$  ratios are  $\sigma_5/\sigma_4 \approx 12.1$  and 5.13 for the no-response and response calculations, respectively.

One can alleviate this ratio inconsistency by normalizing the All  $n$  modeled spectra to the respective experimental area and then scaling the spectral curve in each individual  $n$  capture channel relative to the All  $n$  model rather than using the individual experimental spectra for normalization. We illustrate the result of this alternative process for the

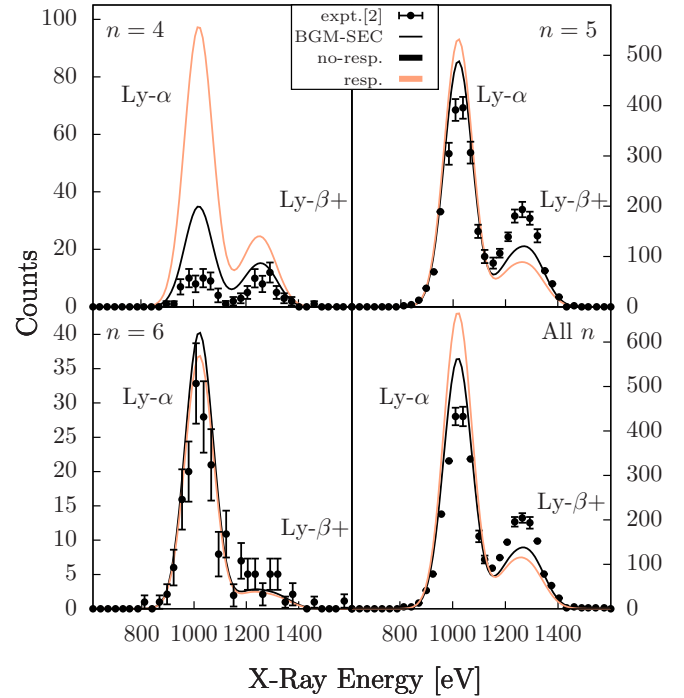


FIG. 7. (Color online) X-ray spectra from SEC in the  $\text{Ne}^{10+}$ -Ne collision system: TC-BGM SEC and experimental data of Ali *et al.* [2]. TC-BGM All  $n$  spectra are normalized to the corresponding experimental area, while modeled spectra for individual  $n$  channels are scaled with respect to the All  $n$  spectra.

$\text{Ne}^{10+}$ -Ne collision system in Fig. 7, where only the TC-BGM spectra are compared to the experimental results. Although the modeled spectra in Fig. 7 are similar in appearance to the ones shown in Fig. 5 for  $n = 5$  and  $n = 6$ , it is clear in Fig. 7 that the area under the TC-BGM spectra for  $n = 4$  is considerably larger than those in Fig. 5. As a result, the ratio of areas under the TC-BGM spectra in Fig. 7 between the  $n = 5$  and the  $n = 4$  channel is now approximately 12.3 and 5.19 for the no-response and response models, respectively. Even though these ratios are not identical to the respective  $\sigma_n$  ratios (12.1 and 5.13 for no response and response, respectively) due to the convolution procedure, it is apparent that these area ratios are in better agreement through this normalization process. If Liu *et al.* were to use this alternative normalization process for the  $\text{Ne}^{10+}$ -Ne collision system, the spectra reported in Ref. [15] would have appeared similar in counts as implied by their  $\sigma_{nl}$  values in Table I, which would have led to different conclusions and assessment of their calculations.

#### IV. CONCLUSIONS

We have presented an independent-electron analysis of SEC in  $\text{Ne}^{10+}$ -He, -Ne, and -Ar collisions using the TC-BGM. Capture cross sections obtained from the solution of the single-electron TDSE were used in a hydrogenic radiative cascade model to obtain x-ray emission spectra. In this framework we have explored how different approximations of the electron-electron interaction, in other words, a time-

dependent screening potential compared to the no-response approximation, can lead to different representations of the state-selective capture cross sections.

We have compared our net capture and SEC cross sections with the CTMC and experimental data reported by Ali *et al.* [2] and the TC-AOCC calculation results of Liu *et al.* [15]. Between the two potential models used in the present study, the no-response approximation shows better agreement with the experimental cross sections than the response model. Additionally, the different approximations of the electron-electron interaction used in the present study had no significant influence on the relative x-ray counts. However, the mutual normalization of the individual spectra reported by Ali *et al.* [2] leads to questionable spectral count ratios; masking strong deviations found in the response calculations on relative cross sections. This misrepresentation of x-ray spectra was demonstrated for the TC-BGM calculations by comparing the spectra that use a more consistent normalization process, unmasking these strong deviations. Regardless, it appears that a nonspherical time-dependent screening model would be necessary to improve on the response results. Furthermore, between the net capture and the SEC probability there is an overall consistency in the latter results with the CTMC and experimental relative cross sections for all collision systems. The present SEC results are also consistent with the experimental and CTMC x-ray spectra. Overall, this collision study has demonstrated that the use of a consistent multinomial analysis is paramount for capture cross-section calculations in an independent-electron analysis.

#### ACKNOWLEDGMENTS

This research was funded by the Natural Sciences and Engineering Research Council of Canada (NSERC) under Grant No. RGPIN-2014-03611. High-performance computing resources for this work were provided through SHARCNET. A.C.K.L. gratefully acknowledges the financial support provided by the Ontario Graduate Scholarship, which is jointly funded by the Province of Ontario and York University (Canada).

#### APPENDIX A: CROSS-SECTION DATA

The  $nl$ -state-selective cross sections from the TC-BGM calculation using the target response model for the electron-electron interaction are listed in Table II. In Sec. III A, relative cross sections from the present calculations, Liu *et al.* [15], and Ali *et al.* [2] are shown in Fig. 3. Table III lists the numerical results shown in that figure.

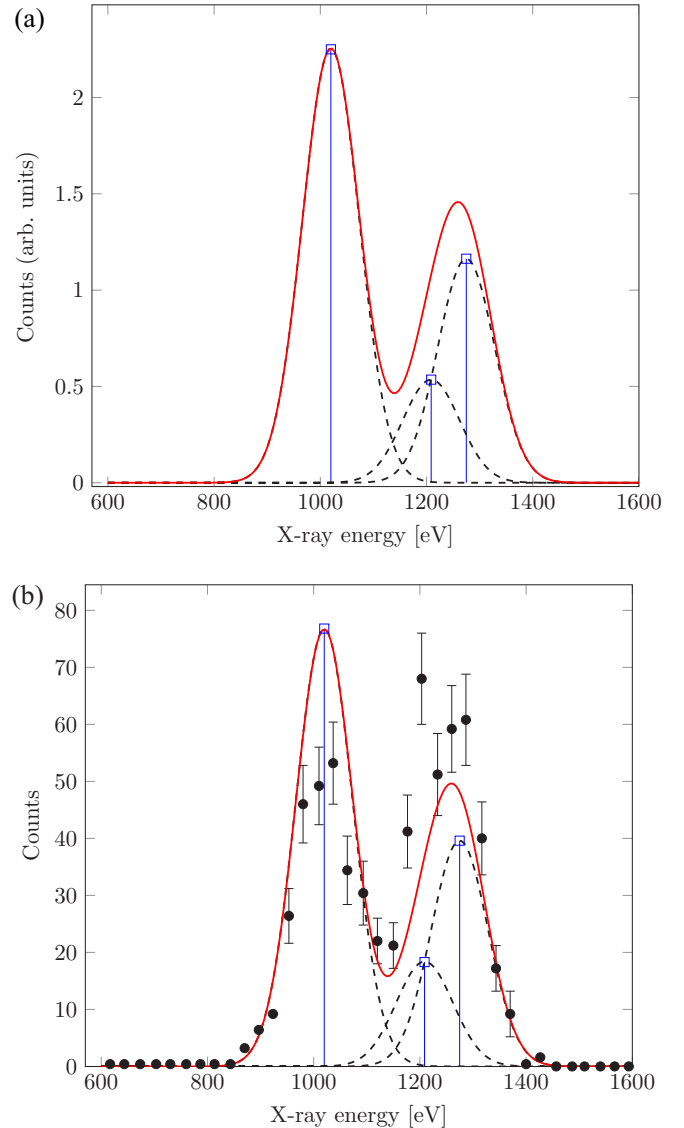


FIG. 8. (Color online) Convolution process of x-ray spectra for  $\text{Ne}^{10+}$ -He collisions and capture into  $n = 4$ : (a) spectral line convolution to Gaussian profiles; (b) overall spectral profile normalized to the experimental area.

#### APPENDIX B: SPECTRAL LINE CONVOLUTION

Figure 8 illustrates the convolution process of the x-ray spectra shown in Sec. III B. The process begins with the calculated photon counts calculated using (9) and plotted with respect to the corresponding x-ray energy for the Lyman series. Each spectral line is given a Gaussian form with a 126-eV FWHM. The Gaussians are summed together to give the overall spectral profile [Fig. 8(a)], and finally, the overall spectral profile is normalized to the area given by the experimental data of Ali *et al.* [2] [Fig. 8(b)].

TABLE II. Partial capture cross sections  $\sigma_{nl}$  (in  $10^{-16}$  cm<sup>2</sup>) from the TC-BGM response model.

States ( $n,l$ )	Ne <sup>10+</sup> -He		Ne <sup>10+</sup> -Ne		Ne <sup>10+</sup> -Ar	
	Net	SEC	Net	SEC	Net	SEC
3,0	0.04161	0.00712	2.396	0.043	3.131	0.002462
3,1	0.08004	0.01303	5.967	0.099	9.640	0.011226
3,2	0.04956	0.00857	9.332	0.154	12.870	0.031634
4,0	1.640	0.400	1.533	0.2218	2.576	0.0663
4,1	5.129	1.101	4.683	0.4429	8.105	0.1621
4,2	7.494	1.524	8.645	0.7607	12.962	0.2984
4,3	6.168	1.200	14.252	1.3187	14.657	0.3618
5,0	0.946	0.471	0.917	0.7508	2.006	0.319
5,1	2.787	1.618	2.734	1.3718	6.181	0.664
5,2	5.201	3.228	5.808	2.5852	10.269	1.091
5,3	8.466	4.815	10.514	4.0832	17.110	1.586
5,4	7.529	4.610	14.895	5.2729	22.182	1.954
6,0	0.063	0.009	0.099	0.0132	1.579	0.852
6,1	0.147	0.024	0.240	0.0284	4.383	1.593
6,2	0.158	0.026	0.371	0.0609	7.433	2.970
6,3	0.266	0.050	0.439	0.1277	12.325	4.628
6,4	0.447	0.110	0.710	0.2540	19.145	6.463
6,5	0.368	0.129	0.808	0.3755	23.628	6.958
7,0	0.00517	0.00118	0.038	0.0013	0.236	0.054
7,1	0.01367	0.00291	0.098	0.0034	0.577	0.116
7,2	0.02133	0.00400	0.151	0.0054	0.926	0.251
7,3	0.02093	0.00485	0.166	0.0057	1.399	0.492
7,4	0.02831	0.00630	0.151	0.0051	2.037	0.960
7,5	0.02516	0.00600	0.148	0.0047	2.999	1.766
7,6	0.01791	0.00496	0.110	0.0057	4.518	2.357

TABLE III.  $n$ -state-selective relative capture cross sections  $\sigma_n^{\text{rel}}$  (in %) for collisions of Ne<sup>10+</sup> with He, Ne, and Ar targets. Experimental and CTMC data [2] along with results of Liu *et al.* [15] and TC-BGM calculations are listed. No-response and response models for TC-BGM calculations are tabulated separately.

$n$	Expt. [2]	CTMC [2]	Liu <i>et al.</i> [15]	TC-BGM IEM: no-response approx.		TC-BGM IEM: target response	
				Net	SEC	Net	SEC
Collision: Ne <sup>10+</sup> -He							
4	18.6	16.4	30.9	34.8	20.3	43.3	21.8
5	78.9	78.4	64.2	60.9	77.6	52.9	76.1
6	2.5	3.8	4.2	3.8	1.2	3.1	1.8
Collision: Ne <sup>10+</sup> -Ne							
4	1.7	2.7	21.7	42.3	7.2	34.0	15.2
5	91.8	88.6	24.4	47.3	86.9	40.7	78.1
6	6.5	8.4	14.2	4.3	5.8	3.1	4.8
Collision: Ne <sup>10+</sup> -Ar							
5	7.4	1	—	38	3.1	28	15.4
6	85.6	77.1	—	43.2	73	33.2	64.4
7	7.0	20.5	—	6.4	22.7	6.2	16.5
8	—	1.1	—	1.6	0.19	0.88	0.29

- [1] R. Ali, P. A. Neill, B. Beiersdorfer, C. L. Harris, M. J. Rakovic, J. G. Wang, D. R. Schultz, and P. C. Stancil, *Astrophys. J. Lett.* **629**, L125 (2005).
- [2] R. Ali, P. A. Neill, P. Beiersdorfer, C. L. Harris, D. R. Schultz, and P. C. Stancil, *Astrophys. J. Lett.* **716**, L95 (2010).
- [3] P. Beiersdorfer, L. Schweikhard, P. Liebisch, and G. V. Brown, *Astrophys. J. Lett.* **672**, 726 (2008).
- [4] T. E. Cravens, *Geophys. Res. Lett.* **24**, 107 (1997).
- [5] J. B. Greenwood, I. D. Williams, S. J. Smith, and A. Chutjian, *Phys. Rev. A* **63**, 062707 (2001).
- [6] V. A. Krasnopolsky, D. J. Christian, V. Kharchenko, A. Dalgarno, S. J. Wolk, C. M. Lisse, and S. A. Stern, *Icarus* **160**, 437 (2002).
- [7] V. Kharchenko, M. Rigazio, A. Dalgarno, and V. A. Krasnopolsky, *Astrophys. J. Lett.* **585**, L73 (2003).
- [8] S. Otranto and R. E. Olson, *Phys. Rev. A* **77**, 022709 (2008).
- [9] S. Otranto, N. D. Cariatore, and R. E. Olson, *Phys. Rev. A* **90**, 062708 (2014).
- [10] M. Fogle, D. Wulf, K. Morgan, D. McCammon, D. G. Seely, I. N. Draganić, and C. C. Havener, *Phys. Rev. A* **89**, 042705 (2014).
- [11] R. Dörner, V. Mergel, O. Jagutzki, L. Spielberger, J. Ullrich, R. Moshhammer, and H. Schmidt-Böcking, *Phys. Rep.* **330**, 95 (2000).
- [12] E. Y. Kamber, M. A. Abdallah, C. L. Cocke, and M. Stöckli, *Phys. Rev. A* **60**, 2907 (1999).
- [13] M. A. Abdallah, C. L. Cocke, W. Wolff, H. E. Wolf, and M. Stöckli, *Phys. Rev. A* **63**, 024702 (2001).
- [14] W. Fritsch and C. D. Lin, *Phys. Rev. A* **54**, 4931 (1996).
- [15] L. Liu, J. G. Wang, and R. K. Janev, *Phys. Rev. A* **89**, 012710 (2014).
- [16] T. Kirchner, H. J. Lüdde, and R. M. Dreizler, *Phys. Scripta* **1999**, 416 (1999).
- [17] M. Horbatsch, *Phys. Lett. A* **187**, 185 (1994).
- [18] D. R. Schultz, R. E. Olson, C. O. Reinhold, S. Kelbch, C. Kelbch, H. Schmidt-Böcking, and J. Ullrich, *J. Phys. B* **23**, 3839 (1990).
- [19] T. Kirchner, M. Horbatsch, H. J. Lüdde, and R. M. Dreizler, *Phys. Rev. A* **62**, 042704 (2000).
- [20] T. Kirchner, M. Horbatsch, and H. J. Lüdde, *Phys. Rev. A* **66**, 052719 (2002).
- [21] A. Salehzadeh and T. Kirchner, *J. Phys. B* **46**, 025201 (2013).
- [22] M. Zapukhlyak, T. Kirchner, H. J. Lüdde, S. Knoop, R. Morgenstern, and R. Hoekstra, *J. Phys. B* **38**, 2353 (2005).
- [23] E. Engel and S. H. Vosko, *Phys. Rev. A* **47**, 2800 (1993).
- [24] O. J. Kroneisen, H. J. Lüdde, T. Kirchner, and R. M. Dreizler, *J. Phys. A: Math Gen.* **32**, 2141 (1999).
- [25] M. M. Sant'Anna, E. C. Montenegro, and J. H. McGuire, *Phys. Rev. A* **58**, 2148 (1998).
- [26] C. Montanari and J. E. Miraglia, *J. Phys. B* **45**, 105201 (2012).
- [27] T. Kirchner, L. Gulyás, H. J. Lüdde, E. Engel, and R. M. Dreizler, *Phys. Rev. A* **58**, 2063 (1998).
- [28] H. Friedrich, *Theoretical Atomic Physics* (Springer, Berlin, 2005).
- [29] S. M. Younger and W. L. Wiese, *Phys. Rev. A* **17**, 1944 (1978).